Journal of Power Sources 244 (2013) 80–86

Contents lists available at SciVerse ScienceDirect

Journal of Power Sources

journal homepage: www.elsevier.com/locate/jpowsour

Composite materials based on polymer-derived SiCN ceramic and disordered hard carbons as anodes for lithium-ion batteries

Monika Wilamowska [a,b], Magdalena Graczyk-Zajac [a,*], Ralf Riedel [a]

[a] Fachbereich Material-und Geowissenschaften, Technische Universität, Petersenstr. 32, 64287 Darmstadt, Germany
[b] Chemical Faculty, Gdansk University of Technology, Narutowicza 11/12, 80-233 Gdansk, Poland

HIGHLIGHTS

- Two kinds of new SiCN ceramic/hard carbons composites were synthesized.
- The electrochemical properties for Li-ion battery application were studied.
- The composites show superior properties to pure hard carbons.
- The composites exhibit a high-recovered capacity and long-life durability.
- The composites are suitable for high power energy devices.

ARTICLE INFO

Article history:
Received 27 October 2012
Received in revised form
20 March 2013
Accepted 22 March 2013
Available online 2 April 2013

Keywords:
Hard carbons
SiCN ceramic
Composite anode materials
Lithium-ion batteries

ABSTRACT

New composite materials based on polymer-derived SiCN ceramics and hard carbons were studied in view of its application as anodes for lithium-ion batteries. Two kinds of composites were prepared by pyrolysis of the preceramic polysilazane (HTT1800, Clariant) at 1000 °C in Ar atmosphere mixed with hard carbons derived from potato starch (HC_PS) or with a hard carbon precursor, namely potato starch (PS), denoted as HTT/HC_PS and HTT/PS composites, respectively. Thermal gravimetric analysis suggests possible reactions between the preceramic polymer and the carbon precursor. The HTT/PS composites contain higher amount of oxygen and appear to be more homogeneous than that of the HTT/HC_PS composite. Raman analysis confirms the presence of highly disordered carbon in the composites by the appearance of the well-pronounced D band at 1347 cm^{-1}. The materials are amorphous with a significant fraction of single graphene sheets as confirmed by X-ray diffraction. The HTT/PS composite exhibits a high-recovered capacity (434 mAh g^{-1} when charging with a current of 36 mA g^{-1}) and outstanding cyclability for 400 cycles even at high current rates (90 mAh g^{-1} when charging with 3600 mA g^{-1}). These properties make the composite a candidate anode material for high power energy devices.

1. Introduction

Carbonaceous materials have been widely used as negative electrodes for lithium-ion batteries [1–6]. Although a huge variety of carbons were tested, an intensive research is still devoted to this class of materials. Graphite provides stability and safety but the capacity does not exceed the theoretical value of 372 mAh g^{-1}. Graphite also does not fulfill the requirements for high power energy devices because the capacity decreases significantly upon charging/discharging with high currents [7,8]. Disordered carbons have attracted a lot of attention over the last decades because of their high specific capacities in the range between 500 and 700 mAh g^{-1} [5,6,9]. Their electrochemical behavior in terms of lithium insertion/extraction with respect to microstructural features has been analyzed in detail by the group of Dahn [10–13]. It has been stated that hard carbons (HC) are promising anode materials for lithium-ion batteries. Moreover, hard carbons are more suitable for high power energy devices than graphite. This finding is due to the characteristic, more capacitive shape of the charge–discharge curve. The significant part of the charge–discharge curve of HC consists of the region where the potential changes gradually. This is the so called constant current region (CC), which enables fast charging and discharging of the material [14]. For most of the hard carbons the constant voltage (CV) region (plateau) of the charge–discharge curve is also present. The CV region is an origin for high capacity but slows down the charging process. There have been many attempts to

* Corresponding author.
E-mail address: graczyk@materials.tu-darmstadt.de (M. Graczyk-Zajac).

0378-7753/$ – see front matter © 2013 Elsevier B.V. All rights reserved.
http://dx.doi.org/10.1016/j.jpowsour.2013.03.137

minimize the CV region of hard carbons in order to improve their high power performance but unfortunately this is always connected with a loss of the capacity [9,14,15].

Another problem to solve in the case of hard carbons is the high irreversible capacity related to a solid electrolyte interphase (SEI) formation and reactions of lithium ions with surface functional groups [12]. Lithium ions can be also irreversibly trapped in pores of the hard carbons [16]. It has been found that the irreversible lithium consumption connected to SEI formation is proportional to the active surface area (ASA) of the carbons [17]. To minimize the capacity loss different surface modifications of the disordered carbons were investigated [17,18]. Béguin et al. obtained a carbon material with reduced ASA by covering the carbon cloth with a thin film of pyrolytic carbon, which significantly reduced the irreversible capacity by hindering diffusion of lithium ions to active sites [17]. The pretreatment of the hard carbon precursor (*i.e.* dewatering of sucrose) or pyrolysis under modified conditions (*i.e.* under ethylene gas) can also significantly diminish the irreversible capacity of surface functional groups [11].

In this work we focus on the investigation of new composite anode materials based on hard carbons embedded into a SiCN ceramic matrix. It was already found that SiCN/graphite composites exhibit higher capacity and better cycling stability than that of pure graphite. Additionally, the presence of the ceramic part significantly enhances the stability of the composites versus lithium intercalation/extraction processes especially for high current rates [19]. Pure SiCN ceramic derived from the commercially available precursor HTT 1800 contains rather low amount of carbon (17.8 wt.% of C) and consequently exhibits poor conductivity and low capacity. This feature makes low carbon containing SiCN unattractive for battery application. However, the presence of hard carbons dispersed in the SiCN matrix ensures sufficient electrical conductivity. In the present study we used two ways of composite preparation, namely (i) by pyrolysis of HTT 1800 containing hard carbon particles (HTT/HC_PS samples) and (ii) by pyrolysis of HTT 1800 comprised of potato starch (hard carbon precursor, HTT/PS samples). The latter procedure leads to a material with excellent electrochemical performance in terms of lithium insertion/extraction, in particular high cycling stability (more than 400 charge/discharge cycles) and high capacity of 90 mAh g^{-1} recovered with high cycling currents ($C = D = 3600$ mAh g^{-1}). The enhanced electrochemical values are explained by the presence of high amount of single layer graphene formed within the carbon nanostructure.

2. Experimental part

2.1. Preparation of hard carbons and composites

Hard carbons (HC) were obtained by pyrolysis of potato starch (PS) (Aldrich, Germany) under Ar atmosphere. The procedure is as follows: preheating for 60 h at 230 °C (Ar atm.), in order to prevent potato starch from foaming during carbonization [20], heating with the rate 100 °C per hour to the final temperature (800 °C, 900 °C or 1000 °C), holding the final temperature for 1 h and cooling with the rate 150 °C per hour to a room temperature.

The composites were prepared by two methods. In the first method the hard carbons (HC_PS) were dried under vacuum at 80 °C (24 h) and mixed with the commercial liquid ceramic precursor polyorganosilazane $-[Si(CH{=}CH_2)(H){-}NH]_x[Si(CH_3)(H){-}NH]_y-$ (HTT1800, Clariant GmBH, Germany) in a glove box (MBraun, Germany) to form a slurry. The ceramic precursor HTT1800 was stored in a glove box prior to use. The weight ratios between HTT and HC_PS were 2.7:1 and 1:1. The slurry was homogenized for 24 h by mechanical mixing and placed in a quartz crucible. Pyrolysis under argon atmosphere was performed in horizontal Heraeus furnace with alumina tube. The pyrolysis program was the same as for pure hard carbons. At 230 °C the ceramic precursor cross-links. The final temperature for the composites was 1000 °C. In the second method the commercial ceramic precursor (HTT) was mixed with potato starch. PS was dried under vacuum at 80 °C (24 h) prior to mixing with HTT. The weight ratios between HTT and PS were 1:1, 1:3.5 and 1:7.3, respectively. The both pyrolysis procedures (1st and 2nd method) were the same the only difference was in the starting carbon material (1st method – hard carbons (HC_PS), 2nd method – potato starch (PS)) and in the weight ratios between components before pyrolysis. The composites obtained with 1st and 2nd method are labeled as HTT/HC_PS and HTT/PS, respectively.

2.2. Preparation of the electrodes and cells

Synthesized hard carbons and composites powders were ground in a mortar and sieved with 40-μm-sieve mesh. Slurry for preparation of the electrodes consisted of 85 wt.% of active material, 5 wt.% of conducting additive (Carbon Black Super P®, Timcal Ltd., Switzerland), 10 wt.% of a binder (polyvinylidene fluoride PVdF, Solef, Germany) and NMP (*N*-methylpyrolidon, BASF, Germany) as a solvent (approx. 0.3 g of NMP for 1 g of suspension). The slurry was spread on the rough side of a copper foil (10 μm, Copper SE-Cu58 Schlenk Metallfolien GmbH & Co. KG, Germany) using a doctor blade coating technique (the thickness of the wet layer was 60 μm) and dried at 80 °C for 24 h. After drying, the circles (electrodes) of 7 mm in diameter were cut. The weight of electrodes was measured, and then the electrodes were dried under vacuum at 80 °C for 24 h in a Buchi oven and transferred directly to the glove box without contact with air. The active material loading was always between 1.7 and 2.5 mg cm^{-2}.

All the electrochemical measurements were performed in two electrode Swagelok® type cells with active material as a working electrode and lithium foil (99.9% purity, 0.75 mm thickness, Alfa Aesar, Germany) as a counter/reference electrode. High purity solution of 1 M $LiPF_6$ in ethylene carbonate (EC) and dimethyl carbonate of 1:1 weight ratio (LP30, Merck KGaA, Germany) was used as an electrolyte. A quartz filter QMA (Whatman™, UK) was used as a separator.

2.3. Characterization techniques

Hermetically closed cells were electrochemically tested by means of galvanostatic and cyclic voltammetry methods using VMP multipotentiostat (BioLogic Science Instruments, France). Galvanostatic cycling was performed between 3.0 and 0.005 V at different current rates. The same rate was used for the charge (C) and for the discharge (D) processes $C = D$ (1C current corresponds to 360 mA g^{-1}).

Scanning electron microscopy (SEM) images were obtained using the Philips XL30FEG Scanning Electron Microscope. All samples were in the form of powder (ground and sieved with 40 μm mesh) stuck to the sample holder with a carbon tape.

Micro-Raman spectra were recorded on a confocal micro-Raman spectrometer Horiba HR800 (Horiba, Japan) with an Ar ion laser at a wavelength of 514 nm.

X-ray powder diffraction was carried out using a flat-sample transmission geometry on a Bruker D8 Advance using Ni-filtered Cu Kα radiation.

For the chemical analysis of the composites the carbon content was determined by a carbon analyzer (Leco C-200, Leco Corporation, USA). The oxygen and nitrogen contents of the powdered composites were determined by an N/O analyzer (Leco TC-436, Leco Corporation, USA). The silicon fraction was calculated as the

difference to 100% of the sum of the wt.% values of carbon, nitrogen and oxygen, assuming a negligibly small amount of hydrogen in the analyzed samples and no other elements present.

Thermal gravimetric analysis (TGA) measurements were performed using a simultaneous thermal analyzer STA 449C (Netzsch Gerätebau GmbH, Germany) under argon gas atmosphere with a flow rate of 25 $cm^3\,h^{-1}$ in Al_2O_3 crucibles. A heating rate and holding time were the same as for pyrolysis program.

3. Results and discussion

3.1. Structural characterization

Table 1 presents the results of elemental analysis of the synthesized composites based on polymer-derived SiCN matrix containing hard carbons and pure SiCN ceramic as the reference sample. Five composites with different carbon contents were investigated: HTT/PS (1:1), HTT/PS (1:3.5), HTT/PS (1:7.3), HTT/HC_PS (2.7:1), HTT/HC_PS (1:1). The values in brackets denote the weight ratio between components before pyrolysis. The distinct proportions between the components were chosen on the basis of TGA measurements of pure components in order to keep the final ratio of ceramic to hard carbons similar for both types of composites. The amount of free carbon was calculated as the remaining carbon after all silicon atoms have been consumed to be bound to nitrogen (Si_3N_4), oxygen (SiO_2) and to carbon (SiC).

The SiCN/hard carbon composites HTT/HC_PS contain 40 to almost 70% of hard carbons. The composites based on potato starch directly mixed with the preceramic polymer (HTT/PS) contain significantly higher amount of oxygen as compared to the composites based on hard carbons derived from potato starch (HTT/HC_PS). Taking into account that the synthesis is performed under argon atmosphere the oxygen has to originate from the carbon precursor potato starch, which contains oxygen bearing amylopectin and amylose. On the other hand the nitrogen content of the HTT/PS composite is much lower than that of the HTT/HC_PS sample, whereas the silicon content is similar. The Si, O and N ratio suggests that in the HTT/PS composites more Si atoms are bound to oxygen than to N atoms whereas in the HTT/HC_PS the situation is opposite. The analyzed distinct chemical nature of the ceramic matrix of both types of composite is important for the electrochemical performance of the materials.

TGA measurements were performed with the pure ceramic precursor (HTT), pure carbon precursor (potato starch) and the mixture of HTT and potato starch in the weight ratio 1:2, respectively. The dependence of the mass loss with temperature is shown in Fig. 1. HTT, potato starch and the mixture HTT/PS lose 40, 71.3 and 57.3% of mass, respectively.

On the basis of the TGA results one can conclude that crosslinking between the ceramic precursor HTT and the carbon precursor PS occurs. If there were no interaction between these two components the mass loss should be equal to 60.9% instead of the measured 57.3%. The significantly higher amount of oxygen found in the HTT/PS composites in comparison with that of the HTT/HC_PS ceramic (Table 1) is explained by in situ reactions between HTT and potato starch during composite preparation and subsequent pyrolysis.

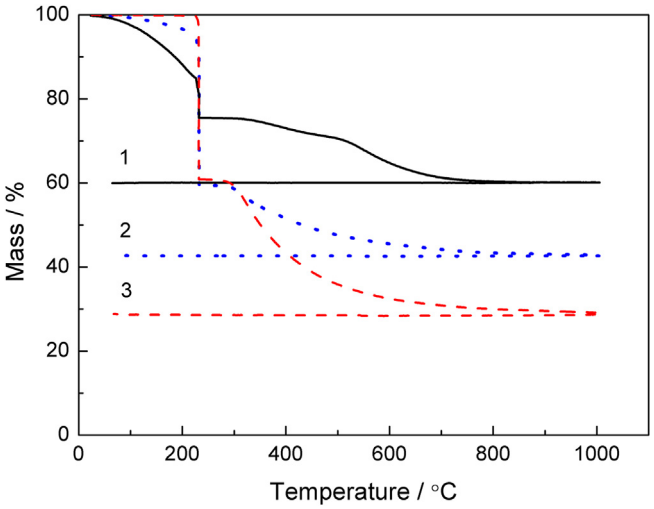

Fig. 1. TGA characteristics of pure ceramic (HTT, solid black line 1), mixture of HTT and PS in the weight ratio 1:2 (HTT/PS (1:2), dotted blue line 2) and potato starch (PS, dash red line 3). (For interpretation of the references to color in this figure legend, the reader is referred to the web version of this article.)

The potato starch contains –OH groups as confirmed by FTIR spectroscopy in the form of the broad band located at 3300–3400 cm^{-1}. Accordingly, the following reaction between the polysilazane HTT and potato starch has to be taken into account [21]:

$$-Si-NH-Si- + 2ROH \rightarrow 2-Si-OR + NH_3$$

This kind of reaction is supported by the results of the elemental analysis: The arithmetically expected amount of nitrogen in the HTT/PS (1:7.3) composite is 5.2 wt% while the measured one accounts 1.6 wt%. Thus, the above-mentioned reaction can explain the decreasing amount of oxygen in the composites.

The amount of oxygen is highest for the composite with the highest ceramic to carbon ratio (HTT:PS 1:1), which suggests that oxygen is bound to silicon. Lower ceramic to carbon ratios do not increase the oxygen content since non-reacted OH groups of the potato starch will be outgassed as CO during pyrolysis.

SEM images of hard carbons and HTT/HC_PS and HTT/PS composites are shown in Fig. 2(a), (b) and (c), respectively. Hard carbons are potato shaped particles of different size, between 6 and 60 μm. The composites differ in terms of morphology. The HTT/HC_PS composite consists of potato shaped particles of hard carbons immersed in the ceramic matrix (Fig. 2(b)), whereas in the case of the HTT/PS composite spherical holes in the ceramic particles can be seen (Fig. 2(c)). The holes appear because of the large mass loss of potato starch (see TGA analysis Fig. 1) during pyrolysis, which causes shrinkage of the carbon particles.

The analysis of the SEM images implies that in contrast to the HTT/HC_PS samples, the composites based on HTT/PS exhibit a pronounced homogeneous microstructure. The morphology of the composites of each type is quite similar for different ratios of the components. For the HTT/PS composite the number of holes increases with increasing ratio of PS to HTT. For the HTT/HC_PS (2.7:1) composite less hard carbon particles are found than for the HTT/HC_PS (1:1) sample.

Table 1
Results of elemental analysis of the investigated composite materials. Values in brackets denote the weight ratio between HTT and hard carbons/hard carbon precursors before pyrolysis.

Weight % composition material	C	O	N	Si[a]	C_{free}
HTT[b]	17.9	2.0	22.3	57.7	8.4
HC_PS	95.5	4.5			
HTT:PS (1:1)	40.9	20.3	9.7	29.0	42.5
HTT:PS (1:3.5)	58.6	16.7	7.0	17.7	61.7
HTT:PS (1:7.3)	69.5	13.6	1.6	15.3	69.1
HTT:HC_PS (2.7:1)	48.0	4.0	13.5	34.5	43.4
HTT:HC_PS (1:1)	62.9	5.7	11.5	19.8	62.9

[a] Calculated as a difference to 100%.
[b] From Ref. [19] prepared at 950 °C.

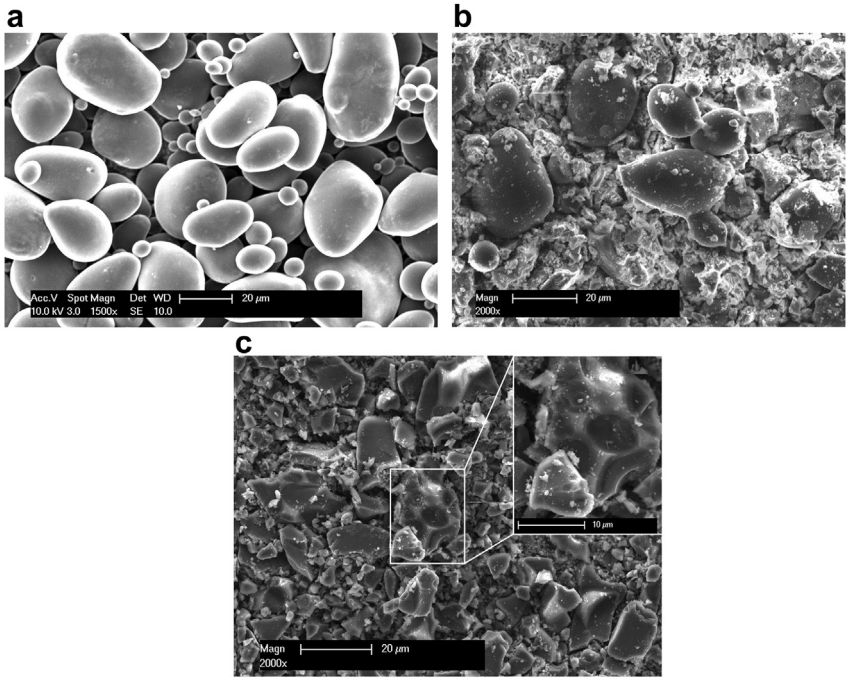

Fig. 2. SEM pictures of (a) hard carbons, (b) HTT/HC_PS (1:1), and (c) HTT/PS (1:7.3) pyrolyzed at 1000 °C.

Micro-Raman spectroscopy was performed in order to determine the structure of the developed carbon phase in the investigated materials. Pure SiCN ceramic (HTT), hard carbons (HC_PS) and both types of composites (HTT/HC_PS and HTT/PS) were analyzed. The resulting Raman spectra are shown in Fig. 3. The pure SiCN ceramic was synthesized at 1100 °C whereas the composites containing hard carbons were produced at 1000 °C in Ar atmosphere. The lower pyrolysis temperature was chosen due to the fact that hard carbons exhibit higher capacity when annealed at temperatures below or equal to 1000 °C [1,22]. In the Raman spectra of all samples two significant bands are present at 1347 cm^{-1} and 1590 cm^{-1}. The values correspond to the D and G bands, respectively, which are typical for carbonaceous materials [23,24]. The D peak results from disorder and defect induced vibration modes of six-fold aromatic carbon rings. Thus, the well-pronounced D band at 1347 cm^{-1} confirms the presence of disordered carbon in all of the investigated materials. The G mode arises from an in-plane bond stretching of sp^2-hybridized carbon atoms [23,25]. Additional bands at 2666 cm^{-1} and 2905 cm^{-1} are found for pure hard carbons. These are namely 2D and D + G bands as shown in Fig. 3, which are attributed to the overtones or the combinations of above-mentioned first order phonon modes [26]. The intensity of the 2D band indicates the degree of organization of the graphene layers. A more intense 2D band goes along with a higher ordering of the graphene sheets in terms of stacking of the layers along the *c*-axis. The significant fluorescence, typical for SiCN ceramic samples prepared at $T \leq 1000$ °C makes a more detailed and quantitative analysis of the Raman spectra impossible.

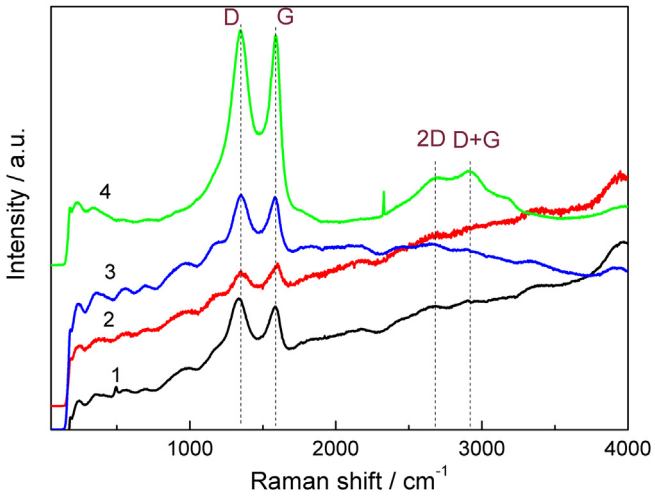

Fig. 3. Raman spectra of pure ceramic SiCN (HTT, black line 1), composites (HTT/PS, red line 2), (HTT/HC_PS, blue line 3) and hard carbons (HC_PS, green line 4); laser wavelength 514 nm. (For interpretation of the references to color in this figure legend, the reader is referred to the web version of this article.)

XRD patterns of the hard carbons, the pure SiCN ceramic (HTT, prepared at 1100 °C) and that of the composites (HTT/HC_PS (1:1) and HTT/PS (1:7.3)) confirm the amorphous nature of the materials (Fig. 4). The XRD patterns of the composites and that of the pure hard carbon are rather similar indicating that the major carbon phase in the composites is disordered carbon. This finding is in agreement with the elemental analysis, which shows that the composites contain 63–69% free carbon. The XRD pattern of the pure SiCN ceramic reveals three broad reflexes, located at 2θ of ~20°, 36.5° and 64.5°. The reflex at ~20° is ascribed to free carbon whereas the reflexes at 36.5° and 64.5° are due to the presence of amorphous or nanocrystalline SiC. The diffraction patterns of hard carbons and that of the composites show a broad reflex at around 23° and a small broad hump at around 43°. There are no reflexes related to nanocrystalline SiC. The peak at $2\theta = 23°$ is the (002) carbon Bragg peak, which gives information about the amount of single, bilayer and trilayer graphene sheets arranged in arbitrary angles [13]. The peak-to-background ratio of the (002) peak is the empirical parameter *R* defined by Liu et al. [13] (see inset in Fig. 4). The smaller the *R* parameter the higher the single layer fraction. The *R* values equal to 1.19, 1.22 and 1.24 were analyzed for HC, HTT/HC_PS and HTT/PS, respectively. The values indicate that the highest fraction of single graphene layers is present in the pure hard carbons in comparison

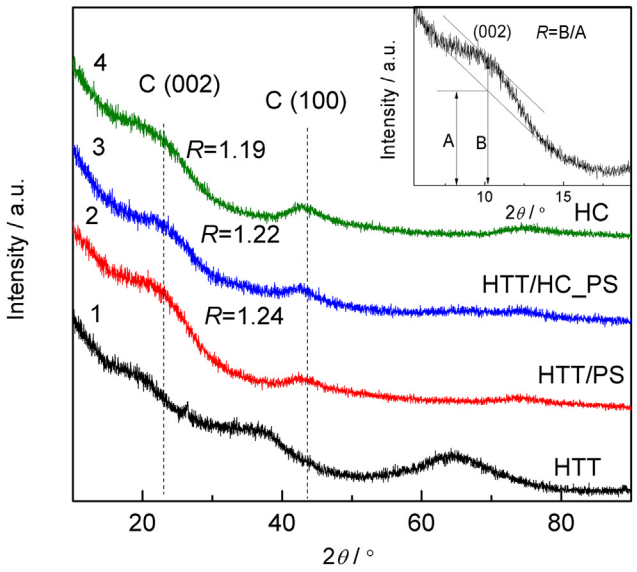

Fig. 4. XRD patterns of pure ceramic SiCN (HTT, black line 1), composites HTT/PS (red line 2), HTT/HC_PS (blue line 3) and hard carbons (HC_PS, green line 4). Inset: the definition of the parameter *R*. (For interpretation of the references to color in this figure legend, the reader is referred to the web version of this article.)

with the composites. Consequently, the composites are characterized by a more ordered carbon phase. However, in the case of the investigated samples the differences between the *R* values are small suggesting the presence of similar structure of single layer graphenes in both the hard carbons and the composites.

3.2. Electrochemical study

Extended cycling performance of electrodes made of hard carbons pyrolyzed at 800 °C, 900 °C and 1000 °C are shown in Fig. 5. The highest capacity was obtained for hard carbons pyrolyzed at 1000 °C. Hard carbon electrodes exhibit stable cycling behavior even when charged and discharged with high current rates (inset in Fig. 5).

The recovered capacity values of the investigated hard carbon electrodes are similar to that of graphite electrodes. The main disadvantage of hard carbons is their high irreversible capacity caused by solid electrolyte interphase (SEI) formation and irreversible reactions between surface functional groups and lithium ions during the insertion process [12]. Covering hard carbons with an inert ceramic polymer is supposed to decrease the irreversible capacity in two ways: (i) by decreasing the active surface area of the HC and (ii) by decreasing a number of surface functional groups of HC since surface functional groups may react with the ceramic precursor during the cross-linking and pyrolysis process.

A comparison of the discharge capacities of all synthesized composites and pure hard carbons is shown in Fig. 6(a). It can be seen that the highest capacity (more than 500 mAh g^{-1} for C/20 rate) was obtained for the composite HTT/PS (1:7.3). This composite contains the highest amount of free carbon (~69 wt%). However, the composite HTT/HC_PS (1:1) which contains a comparable amount of free carbon (~63 wt%) exhibits a much lower capacity (less than half of the capacity obtained for HTT/PS (1:7.3)). A similar situation is found for the composites HTT/PS (1:1) and HTT/HC_PS (2.7:1). Despite a comparable amount of free carbon (42.5 vs. 43.4 wt%, respectively) the capacity of the composite based on carbon precursors (HTT/PS (1:1)) is significantly higher than that of the composite based on hard carbon particles HTT/HC_PS (2.7:1). These results clearly demonstrate that the amount of free carbon is not the only factor which determines the capacity of the electrode material. The carbon microstructures as well as the distribution of

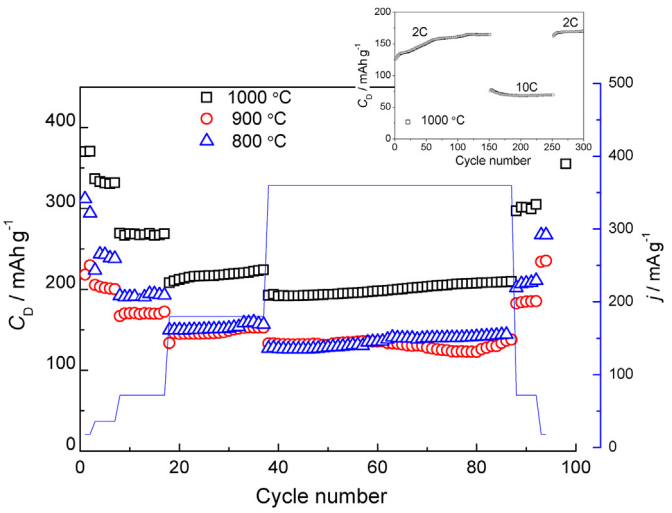

Fig. 5. Extended cycling performance of hard carbon electrodes pyrolyzed at 800 °C, 900 °C and 1000 °C. Inset: high rates cycling performance of HC pyrolyzed at 1000 °C.

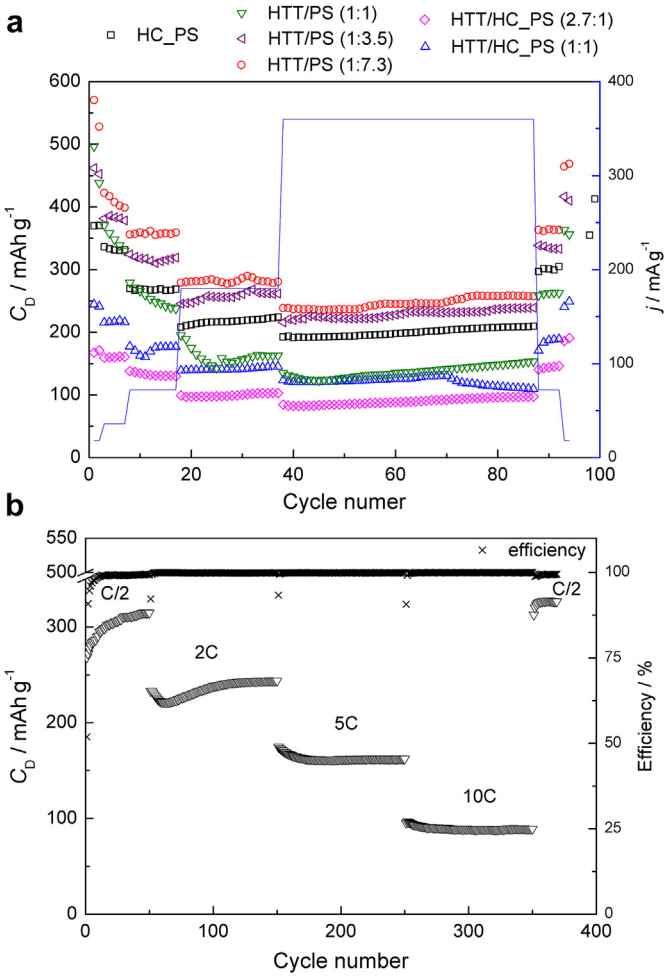

Fig. 6. Extended cycling performance of (a) hard carbons and composites, and (b) HTT/PS (1:7.3) composite cycled with high rates. All materials pyrolyzed at 1000 °C.

the free carbon and the accessibility of the carbon layers for lithium intercalation/extraction are additional important features. The composites HTT/PS contain high amount of oxygen, due to the aforementioned reaction between the preceramic polymer (polysilazane) and the carbon precursor (potato starch) during the pyrolysis process. This pronounced interaction between the components during synthesis changes the composition and microstructure of the ceramic matrix. The presence of oxygen in the potato starch results in the formation of a Si(O)CN ceramic network. It has been found that a significant amount of oxygen in the SiOC structure leads to an increase of both reversible and irreversible capacity of the material [27]. Therefore, the presence of oxygen containing storage sites has to be discussed to be one of the reasons for the enhanced reversible/irreversible capacity of the HTT/PS sample series in comparison to the low oxygen containing HTT/HC_PS materials.

The composite HTT/PS (1:7.3), which exhibits the highest capacity among the investigated materials, is also stable upon cycling with high currents (Fig. 6b). The recovered capacity values obtained for charging/discharging with 5C and 10C rates are equal to 235 and 90 mAh g^{-1}, respectively. Moreover, the capacity does not fade upon cycling and exceeds 300 mAh g^{-1} for a C/2 charge/discharge rate after 400 cycles. The Coulomb efficiency, except for the first few cycles, varies between 99.8 and 100%.

For easier comparison of the electrochemical performance of all the investigated materials, the values of the irreversible (C_{irrev}) and reversible (C_{rev}) capacity of the first cycle (recovered with a rate C/20, the current rates are predefined in Section 2) and the average discharge capacity for different current rates are summarized in Table 2. The capacity values recovered for ceramic/graphite composites (HTT/SLP50 [19]) are also included for reference. The average delithiation capacity C_{av} for C/x charging rate has been calculated as the arithmetic average of the recovered capacity C with n-cycles according to Eq. (1).

$$C_{av} = \frac{\sum_{i=1}^{n} c_i}{n} \quad (1)$$

Embedding of hard carbons into the ceramic matrix does not diminish the irreversible capacity of the composites. The highest C_{irrev} value was obtained for the HTT/PS (1:1) composite, which contains the highest amount of oxygen among the investigated materials.

Nevertheless, we found that the values of the recovered capacity for the HTT/PS (1:7.3) composite are much higher than for pure hard carbons (Table 2). Moreover, the capacity recovered by the HTT/PS (1:7.3) material with 2C/2D current rates is much higher than that of HTT/SLP50 composite, namely 235 mAh g^{-1} vs. 101.8 mAh g^{-1}, respectively. Apparently, the ceramic phase influences the structure of the carbon phase and makes it more accessible for lithium intercalation.

Table 2
Comparison of the irreversible C_{irrev} and reversible capacity C_{rev} of the first cycle and average delithiation capacity of pure hard carbons and composite electrodes compared to values reported for SiCN/graphite ceramic composites [19] derived from different current rates[a].

Capacity (mAh g^{-1})	C_{irrev}	C_{rev}	Average discharge capacity (mAh g^{-1})					
			C/10	C/5	C/2	C	2C	10C
Material								
HC_PS	193	370	333	268	217	200	169	70
HTT:PS (1:7.3)	367	570	434	358	282	246	235	90
HTT:PS (1:3.5)	375	462	382	317	257	229	200	83
HTT:PS (1:1)	623	497	349	254	162	137	190	42
HTT:HC_PS (2.7:1)	180	167	160	133	99	90	62	19
HTT:HC_PS (1:1)	278	244	216	172	141	121	118	34
HTT:SLP50 (1:1)[b]	135	335	324	312	267	166	102	

[a] Current rates are defined in Section 2.
[b] From Ref [19], composite with SLP graphite prepared at 1100 °C.

Fig. 7 presents a comparison of the first charging/discharging curves of pure hard carbons, HTT/HC_PS (1:1) and HTT/PS (1:7.3) electrodes.

The irreversible capacity of hard carbons is related to two contributions. First, of about 50–120 mAh g^{-1} of C_{irr}, for pure hard carbon and HTT_PS (1:7.3), respectively, is due to a SEI formation (usually between 0.7 and 1.2 V). Further irreversible losses during first lithiation are attributed to reactions of lithium with surface functional groups or absorbed molecules that result from exposing the sample to air after pyrolysis [11]. These features correspond to the irreversible capacity between 0.8 and 0.2 V in Fig. 7.

The first charge–discharge curve of the HTT/PS (1:7.3) composite shows two plateau regions. The "sloping plateau" below 0.17 V disappears after the first cycle. This plateau is typical for the lithium intercalation between turbostatically disordered graphene sheets, more characteristic for soft (graphitizing) carbons [11]. The second "quasi-plateau" at very low voltage (<100 mV) is typical for hard carbon electrodes and is ascribed to lithium atoms stored in the pores of hard carbons forming a cluster-like structure. This mechanism is expected to give weakly bound lithium adsorbed at both sides of single graphene layers and in pores formed by graphene layers [11,13,21,28]. In the case of HTT/PS composites this plateau disappears after few cycles. It is possible that lithium ions are trapped in the pores. The constant voltage (CV) region is a source of higher capacity. However, for the high power energy application fast charge–discharge rates are required, so that the CV region is not desired [14]. The region of the charge–discharge curve where the potential changes gradually (constant current (CC) region) and which provides high power is reversible for the HTT/PS composites, even for high rates (10 C).

The low voltage plateau (<100 mV) is analyzed for all the samples in Fig. 7, while the one below 0.17 V can be exclusively seen during lithium insertion into the HTT/PS composite. This phenomenon is discussed in the context of the reaction between the two precursors as discussed in the elemental analysis section. Thus, the final material does not contain pure hard carbon, but is rather comprised of a mixture of single layer graphenes embedded in turbostratic carbons.

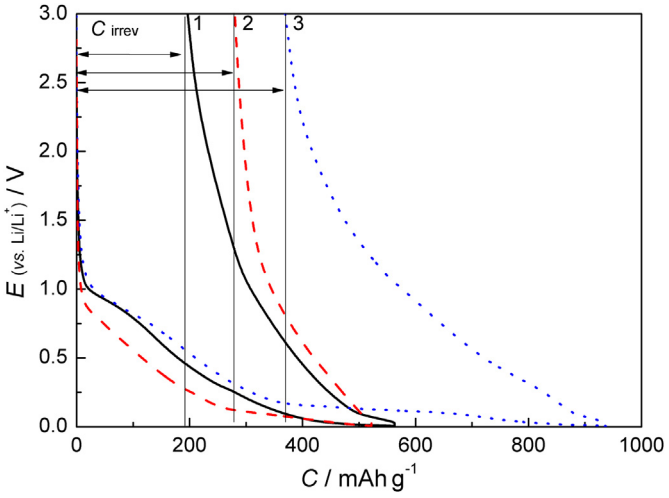

Fig. 7. First lithiation/delithiation cycle of the HC (solid black line 1), HTT/HC_PS (1:1) (dashed red line 2) and HTT/PS (1:7.3) (dotted blue line 3). (For interpretation of the references to color in this figure legend, the reader is referred to the web version of this article.)

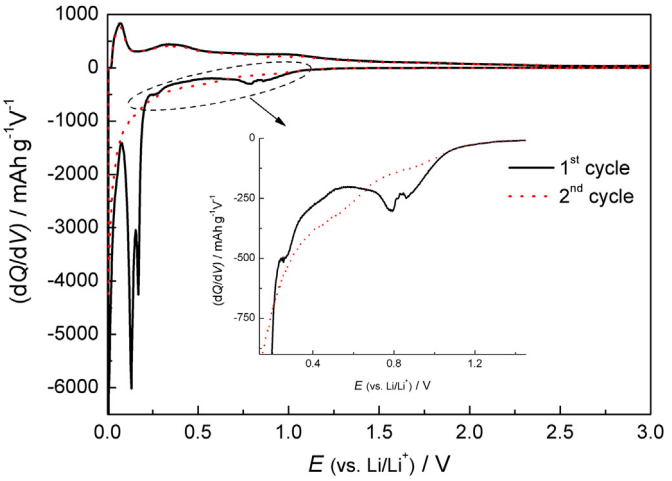

Fig. 8. Differential capacity voltammograms of the first and second cycle for the HTT/PS (1:7.3) composite.

For pure HC and HTT/HC_PS composites only hard carbons are present in the material so that no plateau at higher potential is found. Furthermore, in the case of the HTT/HC_PS composite the interaction between the HC particles and the SiCN ceramic matrix is much weaker than that reported for HTT/graphite composites [19]. As a consequence, the recovered capacity of the HTT/HC_PS composite is comparable to that of pure hard carbon present in the composite. Taking into account that the final HTT/HC_PS composite is composed of 60 wt% HC and 40 wt% SiCN ceramic (calculation based on the HTT1800 mass loss during pyrolysis), agrees with the calculation that 60% of the capacity stems from hard carbons and gives approximately the capacity of HTT/HC_PS material. The main consequence of the presence of the SiCN ceramic in this case is a significant increase in the irreversible capacity.

Potentiodynamic cycling with galvanostatic acceleration was performed for the HTT/PS (1:7.3) composite. The differential capacity voltammogram for the first and second cycle is presented in Fig. 8. It shows the redox state of the system and is in agreement with the galvanostatic curves of the composite. The observed redox peaks correspond well with the plateaus present at the first charge curve. In the first cycle (black solid line, Fig. 8.) the peaks analyzed at 0.87 V and 0.79 V arise from an irreversible reaction of the SEI formation whereas the more pronounced redox peaks at 0.17 V and 0.13 V are related to two stages of lithium insertion into disordered carbons.

4. Conclusions

Composites comprised of polymer-derived SiCN or SiOCN ceramic and hard carbons were synthesized by two methods. In the first method hard carbons obtained from potato starch were used as a source of additional carbon in the composites. In the second method the carbon precursor (potato starch) was used as the carbon source instead of addition of hard carbons. Both types of composites are amorphous materials containing disordered free carbon phase. Mass loss calculated from thermo-gravimetric analysis suggests possible cross-linking reactions between the ceramic precursor and the carbon precursor, which can explain the enhanced oxygen content found in the HTT/PS composites. The HTT/PS composites exhibit a more homogeneous microstructure than that of the HTT/HC_PS composites.

The composites derived from carbon precursors (HTT/PS) exhibit better electrochemical performance and higher capacities than that of the composites prepared by the addition of hard carbon particles to HTT (HTT/HC_PS). Taking into account a comparable amount of free carbon phase in both type of composites this phenomena can be explained by: (i) homogeneous distribution of the carbon phase in the ceramic matrix and/or (ii) presence of single layer graphenes embedded in disordered soft carbons and/or (iii) oxygen containing storage sites in the HTT/PS composites. All synthesized composites exhibit high irreversible capacities, which is the main negative aspect of the materials. Despite quite high irreversible capacity the HTT/PS (1:7.3) composite demonstrates attractive values of recovered capacity (Table 2) and outstanding cyclability for 400 cycles even at high current rates. These properties make this type of composite a promising anode material for high power energy devices.

Acknowledgments

The authors acknowledge the financial support by the Deutsche Forschungsgemeinschaft (DFG), Bonn, Germany within SFB 595/A4 and SPP1473/JP8 programs. M.W. thanks to L.M. Reinold for his help in the experimental work and fruitful discussions. The authors also thank C. Fasel (TGA) and J. Kaspar (elemental analysis) for their support throughout the individual measurements.

References

[1] Z. Ogumi, M. Inaba, in: W.A. van Schalkwijk, B. Scrosati (Eds.), Advances in Lithium-Ion Batteries, Kluwer Academic/Plenum Publishers, New York, 2002, pp. 81–83.
[2] M. Winter, K.-C. Moeller, J.O. Besenhard, in: G.A. Nazri, G. Pistoia (Eds.), Lithium Batteries Science and Technology, Kluwer Academic Publishers, 2004, pp. 144–181.
[3] H. Azuma, H. Imoto, S. Yamada, K. Sekai, J. Power Sources 81–82 (1999) 1–7.
[4] M. Winter, J.O. Besenhard, M.E. Spahr, P. Novák, Adv. Mater. 10 (1998) 725–763.
[5] E. Frackowiak, S. Gautier, F. Leroux, J.N. Rouzaud, F. Béguin, Mol. Cryst. Liq. Cryst. 340 (2000) 431–436.
[6] J.C. Arrebola, A. Caballero, L. Hernán, J. Morales, M. Olivares-Marín, V. Gómez-Serrano, J. Electrochem. Soc. 157 (2010) A791–A797.
[7] T.D. Tran, J.H. Feikert, R.W. Pekala, K. Kinoshita, J. Appl. Electrochem. 26 (1996) 1161–1167.
[8] S.S. Zhang, K. Xu, T.R. Jow, J. Power Sources 160 (2006) 1349–1354.
[9] A. Nagai, K. Shimizu, M. Maeda, K. Gotoh, in: M. Yoshio, R.J. Brodd, A. Kozawa (Eds.), Lithium-Ion Batteries Science and Technologies, Springer Science/Business Media, LLC, 2009, pp. 427–433.
[10] T. Zheng, Y. Liu, E.W. Fuller, S. Tseng, U. von Sacken, J.R. Dahn, J. Electrochem. Soc. 142 (1995) 2581–2590.
[11] E. Buiel, J.R. Dahn, Electrochim. Acta 45 (1999) 121–130.
[12] W. Xing, J.R. Dahn, J. Electrochem. Soc. 144 (1997) 1195–1201.
[13] Y. Liu, J.S. Xue, T. Zheng, J.R. Dahn, Carbon 34 (1996) 193–200.
[14] K. Gotoh, M. Maeda, A. Nagai, A. Goto, M. Tansho, K. Hashi, T. Shimizu, H. Ishida, J. Power Sources 162 (2006) 1322–1328.
[15] K. Shimizu, M. Maeda, S. Morinishi, A. Nagai, A. Hoshi, PTC Int. Appl., (2005) WO/2005/098999.
[16] K. Guérin, A. Ménétrier, S.-M. Février-Bouvier, S. Flandrois, B. Simon, P. Biensan, Solid State Ionics 127 (2000) 187–198.
[17] F. Béguin, F. Chevallier, C. Vix-Guterl, S. Saadallah, V. Bertagna, J.N. Rouzaud, E. Frackowiak, Carbon 43 (2005) 2160–2167.
[18] J.-H. Lee, H.-Y. Lee, S.-M. Oh, S.-J. Lee, K.-Y. Lee, S.-M. Lee, J. Power Sources 166 (2007) 250–254.
[19] M. Graczyk-Zajac, C. Fasel, R. Riedel, J. Power Sources 196 (2011) 6412–6418.
[20] W. Li, M. Chen, C. Wang, Mater. Lett. 65 (2011) 3368–3370.
[21] I. Haiduc, J.J. Zuckerman, Basic Organometallic Chemistry, Walter de Gruyter & Co., Berlin, 1985.
[22] J.R. Dahn, T. Zheng, Y. Liu, J.S. Xue, Science 270 (1995) 590–593. [References cited in the paper].
[23] F. Tuinstra, J.L. Koenig, J. Chem. Phys. 53 (1970) 1126–1130.
[24] A.C. Ferrari, J. Robertson, Phys. Rev. B 61 (2000) 14095–14107.
[25] M.A. Pimenta, G. Dresselhaus, M.S. Dresselhaus, L.G. Canc, A. Jorio, R. Saito, Phys. Chem. Chem. Phys. 9 (2007) 1276–1291.
[26] R.J. Nemanich, S.A. Solin, Phys. Rev. B 20 (1979) 392–401.
[27] D. Larcher, C. Mudalige, A.E. George, V. Porter, M. Gharghouri, J.R. Dahn, Solid State Ionics 122 (1999) 71–83.
[28] K. Tatsumi, J. Conard, M. Nakahara, S. Menu, P. Lauginie, Y. Sawada, Z. Ogumi, Chem. Commun. (1997) 687–688.